Nanoscale

Cite this: *Nanoscale*, 2012, **4**, 6726

www.rsc.org/nanoscale

COMMUNICATION

An aerosol-seed-assisted hybrid chemical route to synthesize anisotropic bimetallic nanoparticles†

Jeong Hoon Byeon[a] and Young-Woo Kim*[b]

Received 24th June 2012, Accepted 19th September 2012
DOI: 10.1039/c2nr31609a

Herein we report the development of anisotropic bimetallic nanoparticles where aerosol gold nanoparticles served as the seeds for the continuous deposition of silver atoms on their surfaces. Initially, aerosol gold nanoparticles were formed by spark discharge and then injected into a silver precursor solution in an impinging device. The gold nanoparticles acted as the seed particles, and catalyzed the reduction of the added silver ions in the presence of ultrasound to yield bimetallic (gold core–silver shell) anisotropic nanoparticles.

Metal nanoparticles are probably the most extensively researched nanomaterials and a frequent tool in nanotechnology. Controlling the shape of nanoparticles is technologically important, since their optical, electronic, magnetic, and catalytic properties often depend critically not only on the particle size, but also on the particle shape.[1–3] The development of synthetic routes for desired single and binary metal nanomaterials has been a great major task for both theoretical and practical applications.[4] For bimetallic nanoparticles, Yang *et al.* mentioned the key parameters such as seeding processes that affect the final shape of products.[5]

Because of attractive plasmon absorption features, the optical properties of bimetallic nanoparticles composed of gold and silver are the subjects of considerable interest in the fields of nanoscience and nanotechnology.[6,7] There have been extensive efforts focusing on the development of new synthetic methodologies of bimetallic nanoparticles with wet chemical processes.[8] Depending on the synthetic procedure, bimetallic nanoparticles can be synthesized homogeneously with the simultaneous reduction of two metal ions or heterogeneously by the successive reduction of two metal ions. The latter type of bimetallic nanoparticles are attracting special attention due to their unique plasmonic properties.[9]

Despite many works on bimetallic nanoparticle preparation, there are no reports on physical methods with the characteristics of being simple, versatile, and green. In this work, we describe our new strategy for the overgrowth on pre-formed aerosol gold nanoparticles. Spark generated aerosol gold nanoparticles were used as seeds for the overgrowth of silver shells in a precursor solution in the presence of ultrasound.

Gold aerosol nanoparticles were produced *via* spark discharge[10,11] and carried by nitrogen gas to an impinging device, as shown in Fig. 1a. A spark discharge is a kind of atmospheric-pressure nonequilibrium discharge.[12] The impinging device, which contained an ultrasound application probe, solutions 1 (silver precursor) and 2 (reducing agent) mixed in the device and an ultrasound probe, was immersed into the mixture solution.[13–15] The aerosol gold nanoparticles experienced ultrasound when they reached the gas (the gold particle laden flow)–liquid (the silver precursor solution in the impinging device) interface. Gold particles in the solution acted as seeds and became kinetically capable of reducing the incoming Ag(I) ions onto the seed particles to create Au–Ag bimetallic configurations. The proposed chemical net reaction on the surface of gold particles in the precursor liquid is as follows:[6]

$$\mathrm{Au_{seed}} + \mathrm{Ag(I)} \xrightarrow{\mathrm{CH_2OH-CH_2OH}} \mathrm{Au_{core} - Ag_{shell}} \qquad (1)$$

During the reaction in liquid phase, silver was deposited through redox chemistry involving the Ag ion, as shown in eqn (1). Silver nuclei which are formed on the surface of the gold particles in the reaction act as the active sites for the further deposition of silver species (Fig. 1b).

The size distributions of aerosol gold nanoparticles were measured using a SMPS, and the results are provided in Fig. 2a. The total number concentration, geometric mean diameter, and geometric standard deviation of the spark generated gold particles were 2.28×10^7 particles per cm^3, 33.6 nm, and 1.51, respectively. Fig. 2b shows the collection efficiency of the gold particles in the impinging device as a function of the ultrasound intensity at 97.4–292.2 W cm^{-2}. At 97.4 W cm^{-2}, aerosol gold particles experienced a force at the gas–liquid interface and about half the particles were collected in the silver precursor solution, because the ultrasound streaming on the interface could give rise to a particle velocity (U_{as}) with the following equation:[16]

$$U_{as} = \left(\frac{2P\beta}{\rho_g c_s \pi \alpha^2 X}\right)^{1/2} \qquad (2)$$

where P is the acoustic power of the ultrasound, β is the acoustic energy attenuation coefficient, ρ_g is the gas density, c_s is the sonic velocity in gas, α is the semi-angle of the spread of the streaming, and

[a]*Department of Chemistry, Purdue University, Indiana 47907, USA*
[b]*Department of Automotive Engineering, Hoseo University, Asan 336-795, Republic of Korea. E-mail: ywkim@hoseo.edu; Fax: +82 41 540 5818; Tel: +82 41 540 5819*

† Electronic supplementary information (ESI) available. See DOI: 10.1039/c2nr31609a

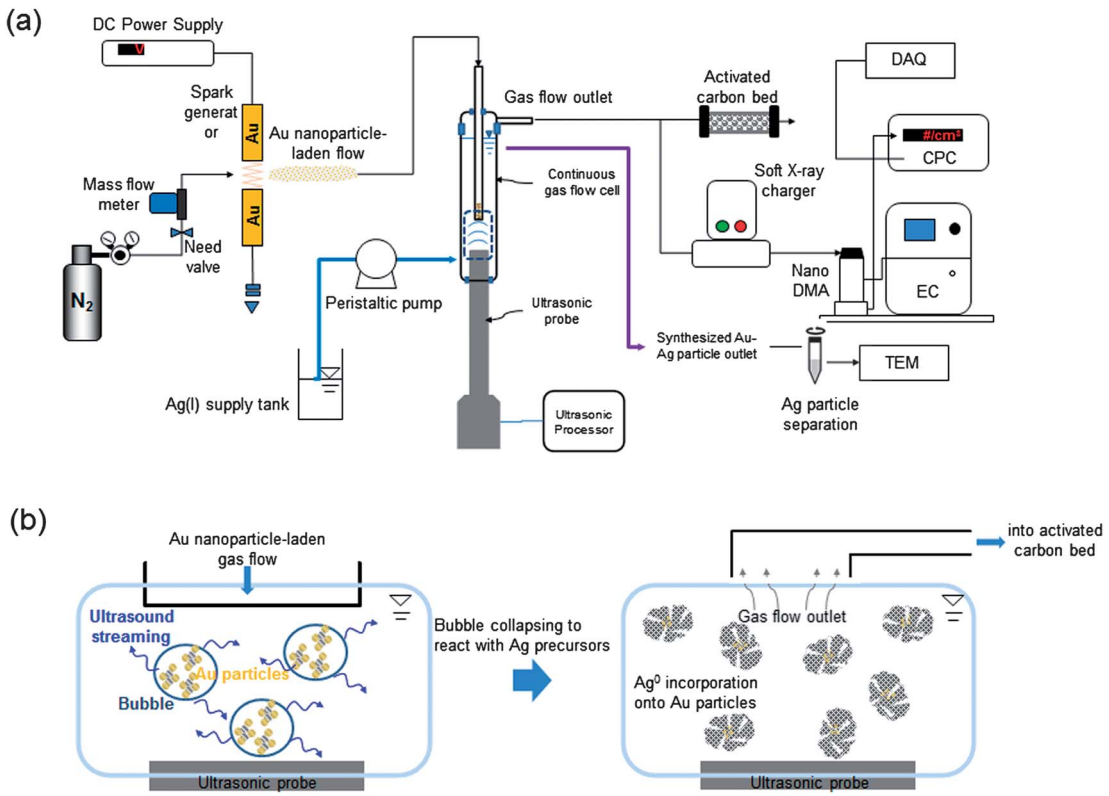

Fig. 1 (a) Schematic diagram of the aerosol-seed-assisted hybrid chemical route used in this work. (b) Scheme of the formation of anisotropic gold–silver particles.

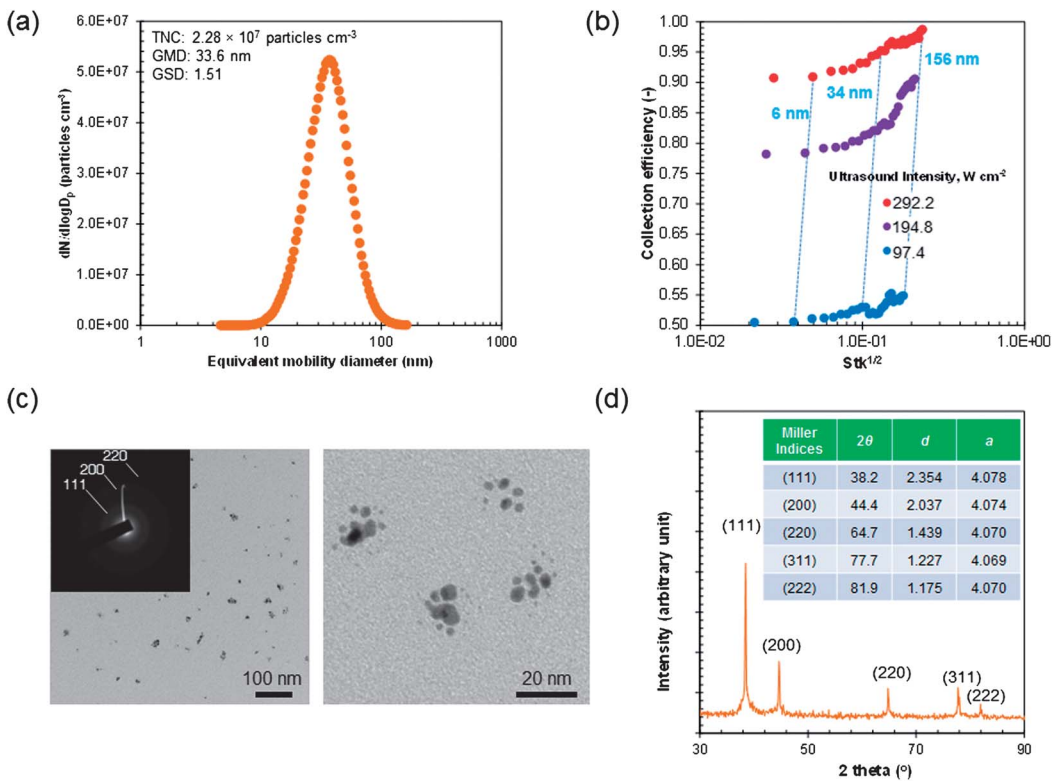

Fig. 2 Results for spark generated aerosol gold nanoparticles. (a) Size distributions of the aerosol gold particles. (b) Collection efficiency of aerosol gold particles in the impinging device with different ultrasound intensities. (c) TEM images of the sampled aerosol gold particles and the ED pattern. (d) XRD pattern of the sampled aerosol gold particles.

X is the distance from the source. Collection efficiencies increased linearly when the Stokes parameter [eqn (3)] increased.[17]

$$\mathrm{Stk}^{1/2} = \left(\frac{C_c \rho_p U_{as} D_p}{9\mu\xi}\right)^{1/2} \quad (3)$$

where Stk is the Stokes number, C_c is the slip correction factor, ρ_p is the particle density, D_p is the particle diameter, μ is the gas viscosity, and ξ is the oscillation amplitude. The same trend was observed for the higher intensities examined in this work, though the collection efficiencies increased. It was expected that the collection efficiency would be a function of the Stokes parameter (from different ultrasound intensities), thus a change in the intensity would not change the shape of the collection efficiency *vs.* the Stokes parameter curve. The collection efficiency of <30 nm particles did not significantly decrease although the particles of <30 nm may be governed by a diffusional motion for the conventional impactors. This may have originated from different mechanisms of the particle attachment on their counter media between the present [the particles in a bubble attached on the liquid surface by bubble collapsing (decreasing bubble sizes from several millimeters to ~2 μm) due to ultrasound streaming] and conventional (the particles in gas attached on a solid plate by inertial impaction) methods.[18] The plots were generated by dividing the output and input aerosol size distributions. The plots show that a decrease in collection efficiency with decreasing size was probably due to a decrease of the attachment frequency between the particle and the liquid surface (*i.e.* increasing distances between the particle and the surface). The morphology and structure of aerosol gold particles were characterized by TEM and electron diffraction (ED). The TEM images (Fig. 2c) revealed that the gold particles were agglomerates of several primary particles (each ~4 nm in diameter). Fig. 2c also shows the ED pattern corresponding to the TEM micrograph. The pattern has a sharp diffraction line showing the (111) reflection and weak diffraction lines showing the (200) and (220) reflections of the face-centered cubic lattice of metallic gold, which indicated that the particles grew predominantly along the (111) lattice and mostly consisted of several nanometer sized crystallites. The XRD (Fig. 2d) of preformed aerosol gold nanoparticles exhibited the following peaks: (111) at $2\theta = 38.2°$, (200) at $2\theta = 44.4°$, (220) at $2\theta = 64.7°$, (311) at $2\theta = 77.7°$, and (222) at $2\theta = 81.9°$. The calculated data for the interplanar spacing d and lattice parameter a are also listed in Fig. 2d.

The deposition of metallic silver on gold particles to form core–shell-structured bimetallic particles is distinctly clear from the difference in contrast between the inner and the outer regions of the particles (Fig. 3a); the lighter regions are invariably a feature of silver. The fast Fourier transformation pattern (also shown in Fig. 3a) of gold–silver particles confirmed the Miller planes (111), 2.35 Å of gold, and (101), 2.42 Å of silver. The increase in particle size with increasing reaction time (*i.e.* an increase in the silver content in the bimetallic particles) can be explained by considering the continuous reduction of silver ions, and as a consequence the particles grew bigger and anisotropic. The competition for the overgrowth on different facets results in anisotropic overgrowth. This anisotropic overgrowth led to flower shape particles. The gold particles effectively acted as seeds to initiate silver deposition. The process was hence clearly observed to occur by the initial nucleation at several sites on the gold followed by growth around these nucleated sites. Fig. 3b shows that the UV-vis spectra exhibited peaks at ~430 nm corresponding to the surface plasmon resonance (SPR) absorption of the particles. The absorption peaks shifted (*i.e.* red shift) from ~405 nm (a typical SPR band of pure silver nanoparticles in the 320–500 nm region with a peak at ~410 nm)[19] to ~430 nm (in the 350–750 nm region, in the present cases). In these cases, where the silver shell is sufficiently thick, a silver SPR peak is mainly observed, demonstrating their relative composition/thickness dependent optical properties.[20] The red shift and broadening of the SPR band in this work were consistent with the fact that the dominant products were Au–Ag bimetallic particles. Moreover, the results (*i.e.* the symmetry of the absorption peak at 0.5 min was better than those at 1.5 and 3.0 min) for 1.5 and 3.0 min also corresponded to an indication of an increase in the size of the silver particles with different shapes as a result of diffusive growth, aggregation, or a combination of

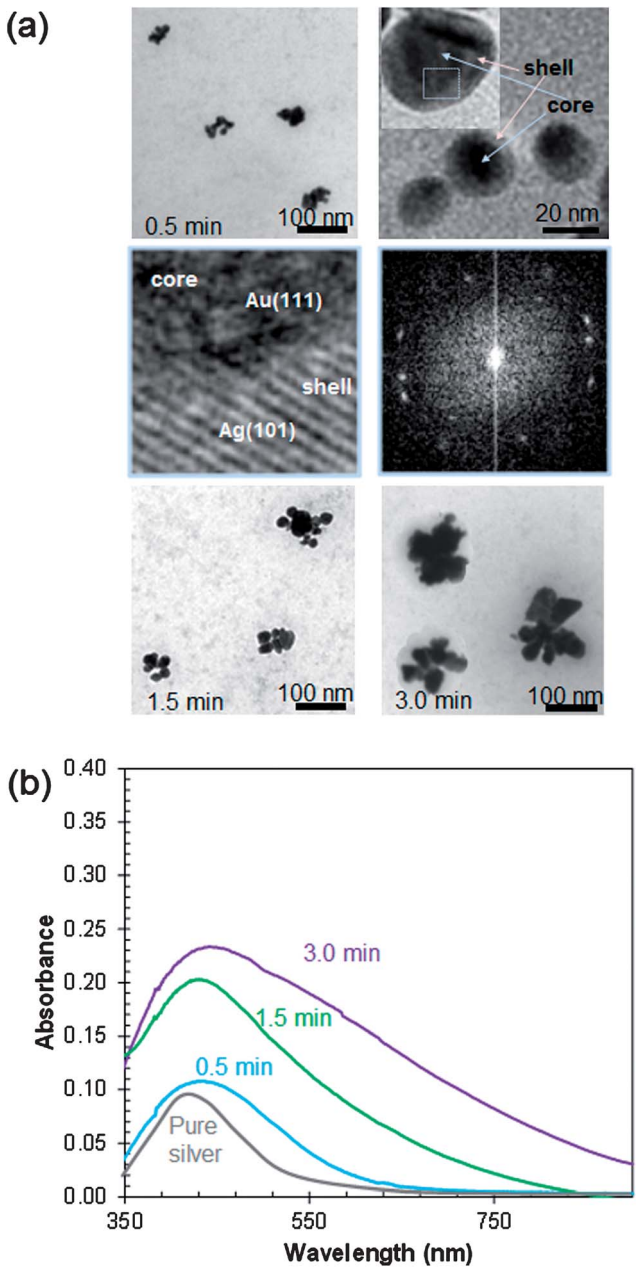

Fig. 3 Results for anisotropic gold–silver particles. (a) TEM images of the anisotropic gold–silver particles at different reaction times and the ED pattern for 0.5 min reaction time. (b) UV-vis spectra of the anisotropic gold–silver particles at different reaction times.

both.[21,22] According to the Mie theory, the position of the SPR band maxima of the particles is sensitive to changes in the refractive index of the embedding medium, as

$$\lambda_{peak}{}^2 = (2\pi c_1)^2 mNe^2(\varepsilon_\infty + 2n^2)/\varepsilon_0 \quad (4)$$

where λ_{peak} is the position of the SPR band, c_1 is the speed of light, m is the effective mass of conduction electrons, N is the free electron concentration, e is the electronic charge, ε_∞ is the optical dielectric function of the metal, and ε_0 is the free space permeability.

The novelty of this hybrid chemical route to prepare anisotropic bimetallic particles lies in its simplicity and simultaneous control of both morphology and size of the particles without any use of a capping agent or template. This process is new, simple, versatile, and environmentally friendly, and this or a modified version may be useful for other systems of nanoparticles for producing bimetallic particles with unique morphologies.

Notes and references

1 M. Banerjee, S. Sharma, A. Chattopadhyay and S. S. Ghosh, *Nanoscale*, 2011, **3**, 5120.
2 J. H. Song, F. Kim, D. Kim and P. Yang, *Chem.–Eur. J.*, 2005, **11**, 910.
3 M. J. Alam and M. Tsuji, *CrystEngComm*, 2011, **13**, 6499.
4 T.-H. Tran and T.-D. Nguyen, *Colloids Surf., B*, 2011, **88**, 1.
5 A. R. Tao, S. Habas and P. Yang, *Small*, 2008, **4**, 310.
6 S. Pande, S. K. Ghosh, S. Praharaj, S. Panigrahi, S. Basu, S. Jana, A. Pal, T. Tsukuda and T. Pal, *J. Phys. Chem. C*, 2007, **111**, 10806.
7 Y. Ji, S. Yang, S. Guo, X. Song, B. Ding and Z. Yang, *Colloids Surf., A*, 2010, **372**, 204.
8 M. Kahraman, Ö. Aydin and M. Çulha, *Plasmonics*, 2009, **4**, 293.
9 K. Mallik, M. Mandal, N. Pradhan and T. Pal, *Nano Lett.*, 2001, **1**, 319.
10 J. H. Byeon, J. H. Park and J. Hwang, *J. Aerosol Sci.*, 2008, **39**, 888.
11 J. H. Byeon and J.-W. Kim, *Thin Solid Films*, 2010, **519**, 700.
12 K. Ostrikov and A. B. Murphy, *J. Phys. D: Appl. Phys.*, 2007, **40**, 2223.
13 J. H. Byeon and Y.-W. Kim, *Ultrason. Sonochem.*, 2012, **19**, 209.
14 J. H. Byeon and J. T. Roberts, *ACS Appl. Mater. Interfaces*, 2012, **4**, 2693.
15 J. H. Byeon and Y.-W. Kim, *Ultrason. Sonochem.*, DOI: 10.1016/j.ultsonch.2012.06.002.
16 S. V. Komarov, S. H. Son, N. Hayashi, S. D. Kaloshkin, O. V. Abramov and E. Kasai, *Surf. Coat. Technol.*, 2007, **201**, 6999.
17 D. S. Kim, K. S. Lim, R. B. Xiang and K. W. Lee, *J. Aerosol Sci.*, 2002, **33**, 1405.
18 D. Park, N.-K. Choi, S.-G. Lee and J. Hwang, *Part. Part. Syst. Charact.*, 2009, **26**, 179.
19 S. Pyne, P. Sarkar, S. Basu, G. P. Sahoo, D. K. Bhui, H. Bar and A. Misra, *J. Nanopart. Res.*, 2011, **13**, 1759.
20 T. Som and B. Karmakar, *Nano Res.*, 2009, **2**, 607.
21 D. A. Andreescu, C. Eastman, K. Balantrapu and D. V. Goia, *J. Mater. Res.*, 2007, **22**, 2488.
22 A. Callegari, D. Tonti and M. Chergui, *Nano Lett.*, 2003, **3**, 1565.